crystals

MDPI

Article

On the Polymorphism of $Cu_2V_2O_7$: Synthesis and Crystal Structure of δ-$Cu_2V_2O_7$, a New Polymorph

Ilya V. Kornyakov [1,2] and Sergey V. Krivovichev [1,2,*]

[1] Department of Crystallography, Institute of Earth Sciences, St. Petersburg State University, University Emb. 7/9, 199034 St. Petersburg, Russia; ikornyakov@mail.ru
[2] Nanomaterials Research Centre, Kola Science Centre, Russian Academy of Sciences, Fersmana 14, 184209 Apatity, Russia
* Correspondence: s.krivovichev@ksc.ru

Abstract: Single crystals of the new modification of copper pyrovanadate, δ-$Cu_2V_2O_7$, were prepared using the chemical vapor transport reaction method. The crystal structure (monoclinic, $P2_1/n$, a = 5.0679(3), b = 11.4222(7), c = 9.4462(6) Å, β = 97.100(6)°, V = 542.61(6) Å^3, Z = 4) was solved by direct methods and refined to R_1 = 0.029 for 1818 independent observed reflections. The crystal structure contains two Cu sites: the Cu1 site in [4+2]-octahedral coordination and the Cu2 site in [4 + 1]-tetragonal pyramidal coordination. There are two V^{5+} sites, both tetrahedrally coordinated by O atoms. Two adjacent $V1O_4$ and $V2O_4$ tetrahedra share the O4 atom to form a V_2O_7 dimer. The crystal structure of δ-$Cu_2V_2O_7$ can be described as based upon layers of V_2O_7 dimers of tetrahedra parallel to the (001) plane and interlined by chains of the edge-sharing $Cu1O_6$ and $Cu2O_5$ polyhedra running parallel to the a axis and arranged in the layers parallel to the (001) plane. The crystal chemical analysis of the three other known $Cu_2V_2O_7$ polymorphs indicates that, by analogy with δ-$Cu_2V_2O_7$, they are based upon layers of V_2O_7 groups interlinked by layers consisting of chains of CuO_n coordination polyhedra (n = 5, 6). The crystal structures of the $Cu_2V_2O_7$ polymorphs can be classified according to the mutual relations between the Cu-O chains, on the one hand, and the V_2O_7 groups, on the other hand. The analysis of the literature data and physical density values suggests that, at ambient pressure, α- and β-$Cu_2V_2O_7$ are the low- and high-temperature polymorphs, respectively, with the phase transition point at 706–710 °C. The β-phase (ziesite) may form metastably under temperatures below 560 °C and, under heating, transform into the stable α-phase (blossite) at 605 °C. The δ- and γ-polymorphs have the highest densities and most probably are the high-pressure phases. The structural complexity relations among the polymorphs correspond to the sequence α = β < γ < δ; i.e., the δ phase described herein possesses the highest complexity, which supports the hypothesis about its stability under high-pressure conditions.

Keywords: copper pyrovanadate; crystal structure; polymorphism; metastability; structural complexity

Citation: Kornyakov, I.V.; Krivovichev, S.V. On the Polymorphism of $Cu_2V_2O_7$: Synthesis and Crystal Structure of δ-$Cu_2V_2O_7$, a New Polymorph. *Crystals* **2024**, *14*, 857. https://doi.org/10.3390/cryst14100857

Academic Editor: Zongyou Yin

Received: 4 September 2024
Revised: 25 September 2024
Accepted: 27 September 2024
Published: 29 September 2024

Copyright: © 2024 by the authors. Submitted for possible open access publication under the terms and conditions of the Creative Commons Attribution (CC BY) license (https://creativecommons.org/licenses/by/4.0/).

1. Introduction

Copper pyrovanadate ($Cu_2V_2O_7$) attracts considerable attention due to its photocatalytic properties, with possible applications in photoelectrochemical water oxidation, size-tunable photoconversion efficiency, chemical sensors, etc. [1–13]. The magnetic properties of α- and β-$Cu_2V_2O_7$ have been the subject of numerous theoretical and experimental studies [14–24]. The α-$Cu_2V_2O_7$ phase is noncentrosymmetric with remarkable multiferroic properties [25–27]. Both the α- and β-modifications of copper pyrovanadate display negative thermal expansion (NTE), which is rarely observed for orthorhombic and monoclinic crystals, respectively [28,29]. Last but not least, α- and β-$Cu_2V_2O_7$ are known as the mineral species blossite and ziesite, respectively, discovered in fumaroles of the Isalco Volcano, Salvador [30–32].

The polymorphism of $Cu_2V_2O_7$ is currently a rather confused issue. The CuO-V_2O_5 system was studied in [33–35] and it was established that the low-temperature α-modification transforms slowly into the β-modification at 712 °C. The subsequent crystal chemical studies revealed basic structural features of both polymorphs, either of synthetic or natural origin [32,36–38]. It was established that the high-temperature β-phase may form metastably if crystallized fast below the $\alpha \rightarrow \beta$ transition temperature, which is considered a major reason for its occurrence as a mineral species in nature. Clark and Garlick [39] reported that, upon heating, the metastable β-phase at 605 °C transforms into the α-phase, which, at 705 °C, transforms into the third phase, γ-$Cu_2V_2O_7$. The same sequence of phase transformations was reported by Petrova et al. [40], who demonstrated that the high-temperature phase at 740 °C is also monoclinic, *C*2/*c*, with unit cell parameters similar to those of the β-phase, which prompted the authors to identify this phase as β′-modification. There are almost no doubts that the β′-phase reported by Petrova et al. [40] is identical to the γ-modification described in [39]. The nomenclature by Clark and Garlick [39] was used in subsequent works [41,42].

Using chemical vapor transport techniques, Krivovichev et al. [43] synthesized another polymorph of $Cu_2V_2O_7$ and determined its crystal structure, which appears to be triclinic and structurally different from those of the α- and β-phases. This triclinic phase was identified as a γ-polymorph, thereby creating the possibility of its confusion with the high-temperature phase reported by Clark and Garlick [39]. The thermodynamic nature of the triclinic polymorph was unclear until 2022, when Turnbull et al. [44] reported the $\beta \rightarrow \gamma$ phase transition induced by rather low pressures (< 0.4 GPa). This observation explained the formation of γ-$Cu_2V_2O_7$ in chemical vapor transport experiments in evacuated silica tubes, where additional pressure may be created by the small amount of water vapor present in the starting chemicals (see, e.g., [45]).

The aim of the present work is threefold. First, we report on the synthesis and crystal structure determination of a novel $Cu_2V_2O_7$ polymorph (termed δ-modification; the phase was synthesized accidentally in a small amount when studying the K-Cu-V-O-Cl system). Second, we analyze the crystal chemical relations between the known $Cu_2V_2O_7$ modifications with particular attention paid to their structural complexity. Third, we attempt to identify the proper relations between the known $Cu_2V_2O_7$ polymorphs, their relative stability, and the recommended nomenclature.

2. Materials and Methods

2.1. Synthesis

Single crystals of δ-$Cu_2V_2O_7$ were prepared using the chemical vapor transport reaction method. Stoichiometric quantities of copper oxide (0.08 g, CuO, 99%, Vekton, St. Petersburg, Russia), vanadium oxide (0.182 g, V_2O_5, 99%, Vekton) and potassium chloride (0.075 g, KCl, 99%, Vekton) were ground together in an agate mortar and the resulting mixture was heated at 250 °C for 24 h in air. The sample was further loaded into a fused quartz ampoule (~12 cm long, a ~0.8 cm inner diameter and a 0.1 cm wall thickness), which was evacuated to a pressure of 10^{-2} mbar and sealed. The ampoule was placed horizontally into a two-zone furnace and heated to 650 °C over 4 h, with a temperature difference of ~50 °C between the source and deposition zones. After 72 h, the ampoule was slowly cooled to 200 °C over the course of 99 h, and then the furnace was turned off. The inner walls of the ampoule were covered by fine crystals of α- and β-$Cu_2V_2O_7$. The source zone contained single crystals of a synthetic analogue of stoiberite, $Cu_5O_2(VO_4)_2$. The walls between the center of the ampoule and the deposition zone contained small and rare, thin, black needles of $K(V_3O_8)$. Additional phases from the K-Cu-V-O-Cl system were discovered via a powder X-ray diffraction study (see below). The end of the ampoule was cracked but unbroken and filled with a mixture of different $Cu_2V_2O_7$ polymorphs, both α- and β- $Cu_2V_2O_7$, with the addition of the γ-polymorph. After close examination under an optical microscope, small, laminar, orange-red crystals were found as intergrowths with

crystals of different $Cu_2V_2O_7$ polymorphs. The single-crystal X-ray diffraction analysis was conducted, which confirmed the novelty of the phase.

2.2. Powder X-ray Diffraction

In order to verify the phase composition of the sample, the crystals from the inner walls of the ampoule were ground in an agate mortar. The resulting polycrystalline powder was then studied using powder X-ray diffraction using a Rigaku Miniflex II diffractometer equipped with a CoKα_{1+2} X-ray tube (λ(CoKα_1) = 1.78896 Å; λ(CoKα_2) = 1.79285 Å). The diffractogram was recorded over a 2θ range of 3–80° with a 0.02° step size and a scan speed of 2 °/min. The sample was rotated during the data collection at a speed of 20 RPM. A phase identification procedure was performed using PDXL 2 software [46] with the implemented ICDD's PDF-2 (release 2020) powder database [47]. The presence of each phase was confirmed by fitting its structural data, imported from ICSD ver. 4.8.0 using the TOPAS 5 software via the Whole Powder Pattern Fitting method [48,49]. The final profile fitting (Figure 1; R_{wp} = 5.55%) included all four polymorphs of $Cu_2V_2O_7$, $K_{0.5}V_2O_5$ [50], $K_4CuV_5O_{15}$ [51] and VOCl [52]. It should be noted that several peaks were not indexed (asterisks in Figure 1) and, therefore, the proper quantitative powder X-ray diffraction analysis could not be carried out. The presence of the new polymorph of $Cu_2V_2O_7$ in the mixture was therefore confirmed by the powder X-ray diffraction study.

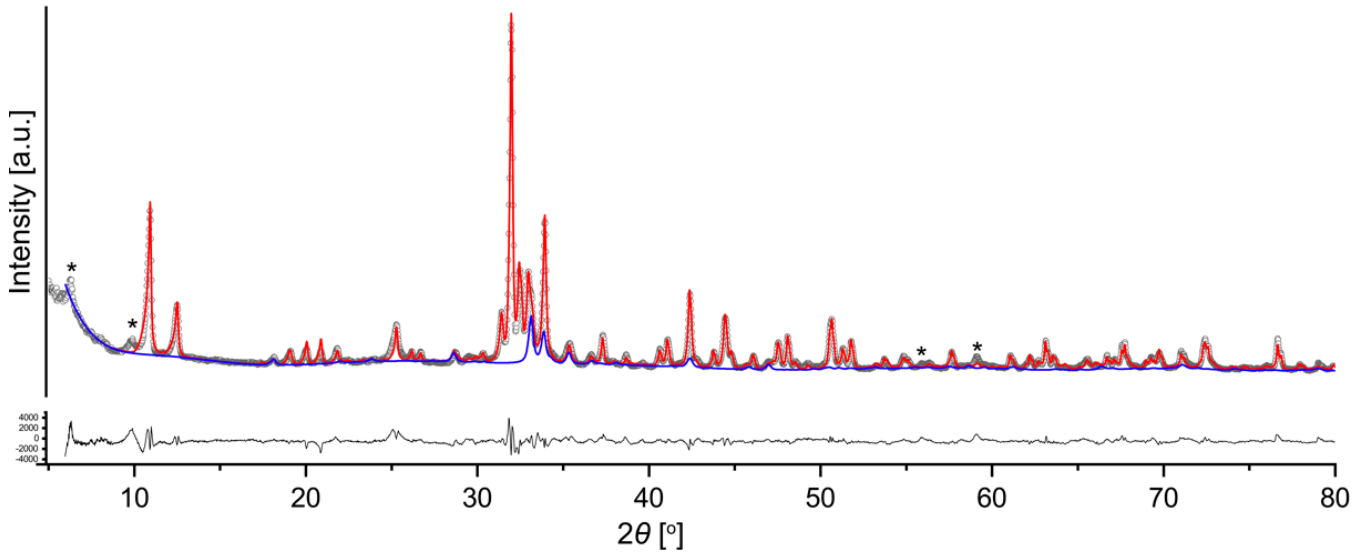

Figure 1. X-ray powder diffraction pattern of the synthesis mixture consisting of all four polymorphs of $Cu_2V_2O_7$, $K_{0.5}V_2O_5$, $K_4CuV_5O_{15}$ and VOCl. The red line shows calculated X-ray diffraction pattern of the whole mixture; the contribution from δ-$Cu_2V_2O_7$ is shown by the blue line; open black circles indicate experimentally measured pattern; asterisks shows peaks of unidentified phases.

2.3. Single-Crystal X-ray Diffraction

A single crystal of δ-$Cu_2V_2O_7$ was selected for the data collection under an optical microscope. For the diffraction experiment, the crystal was coated with an oil-based cryoprotectant and mounted on a cryoloop. The X-ray diffraction study was conducted using a Rigaku XtaLAB Synergy-S X-ray diffractometer operated with a monochromatic microfocus MoKα tube PhotoJet-S at 50 kV and 1.0 mA and equipped with a CCD HyPix 6000HE hybrid photon-counting detector. CrysAlisPro software [53] was used for the integration and correction of the diffraction data for polarization, for background and Lorentz effects, for a numerical absorption correction based on Gaussian integration over a multifaceted crystal model, and for an empirical absorption correction based on spherical harmonics implemented in the SCALE3 ABSPACK algorithm. The unit cell parameters were refined using a least-squares technique. The structure was solved by a dual-space

algorithm and refined using SHELX programs [54] incorporated in the OLEX2 program package [55]. Crystal data, data collection information and structure refinement details are given in Table 1, and atom coordinates and selected interatomic distances are given in Tables 2 and 3, respectively. Table 4 provides the results of the bond valence analysis that shows that all atoms have bond valence sums according to their expected oxidation states.

Table 1. Crystal data and structure refinement for δ-$Cu_2V_2O_7$.

Crystal Data	
Chemical formula	$Cu_2V_2O_7$
M_r	340.96
Crystal system, space group	Monoclinic, $P2_1/n$
Temperature (K)	296(2)
a, b, c (Å)	5.0679(3), 11.4222(7), 9.4462(6)
β (°)	97.100(6)
V (Å^3)	542.61(6)
Z	4
μ (mm^{-1})	11.05
Crystal size (mm^3)	0.04 × 0.03 × 0.01
Data collection parameters	
Diffractometer	Rigaku XtaLAB Synergy-S
Radiation type	Mo$K\alpha$
Absorption correction	Gaussian
T_{min}, T_{max}	0.856, 0.943
Nos. of measured, independent and observed [$I > 2\sigma(I)$] reflections	5290, 1818, 1472
R_{int}	0.037
$(\sin\theta/\lambda)_{max}$ (Å^{-1})	0.777
Refinement parameters	
R_1 [$F^2 > 2\sigma(F^2)$], $wR(F^2)$, S	0.029, 0.059, 1.03
No. of reflections	1818
No. of parameters	100
$\Delta\varrho_{max}$, $\Delta\varrho_{min}$ (e Å^{-3})	0.80, −0.85

Table 2. Atomic coordinates and equivalent isotropic displacement parameters (10^{-4} Å^2) for δ-$Cu_2V_2O_7$.

Atom	***x*/*a***	***y*/*b***	***z*/*c***	U_{iso}
Cu1	0.14483(7)	0.30752(3)	0.43693(4)	0.01026(10)
Cu2	0.87981(7)	0.65745(3)	0.05332(4)	0.01229(10)
V1	0.63692(9)	0.41149(4)	0.20780(5)	0.00787(11)
V2	0.28194(9)	0.62031(4)	0.34339(5)	0.00739(11)
O1	0.8207(4)	0.31193(17)	0.3096(2)	0.0114(4)
O2	0.8307(5)	0.50883(19)	0.1396(3)	0.0215(5)
O3	0.4445(4)	0.34412(17)	0.0733(2)	0.0140(4)
O4	0.4170(4)	0.48002(18)	0.3227(3)	0.0164(5)
O5	0.5059(4)	0.70625(16)	0.4489(2)	0.0114(4)
O6	0.2050(4)	0.68621(16)	0.1763(2)	0.0107(4)
O7	0.0105(4)	0.60076(16)	0.4206(2)	0.0112(4)

Table 3. Selected interatomic distances (Å) for the crystal structure of δ-$Cu_2V_2O_7$.

Cu1—O1	1.913(2)	V1—O1	1.692(2)
Cu1—O5	1.962(2)	V1—O2	1.665(2)
Cu1—O6	1.961(2)	V1—O3	1.689(2)
Cu1—O7	1.947(2)	V1—O4	1.825(2)
Cu1—O3	2.452(2)	<V1—O>	1.718
Cu1—O4	2.705(2)		
<Cu1—O>	2.157	V2—O4	1.763(2)
		V2—O5	1.722(2)
Cu2—O2	1.913(2)	V2—O6	1.748(2)
Cu2—O3	1.909(2)	V2—O7	1.650(2)
Cu2—O5	1.990(2)	<V2—O>	1.721
Cu2—O6	1.924(2)		
Cu2—O1	2.480(2)		
<Cu2—O>	2.043		

Table 4. Bond valence analysis (v.u.: valence units) for the crystal structure of δ-$Cu_2V_2O_7$ *.

Atom	O1	O2	O3	O4	O5	O6	O7	S
Cu1	0.53		0.12	0.06	0.46	0.46	0.48	2.11
Cu2	0.11	0.53	0.54		0.43	0.51		2.11
V1	1.32	1.41	1.33	0.94				4.99
V2				1.10	1.22	1.14	1.47	4.93
S	1.96	1.94	2.09	2.10	2.11	2.11	1.95	

* Calculated using bond valence parameters from [56].

3. Results

3.1. Cation Coordination

The crystal structure of δ-$Cu_2V_2O_7$ contains two Cu sites (Figure 2a). The Cu1 site is in [4 + 2]-octahedral coordination with four short (1.913–1.962 Å) and two long (2.452 and 2.705 Å) Cu1-O bonds. This kind of distortion is typical for Cu^{2+} ions coordinated by oxygen and is due to the Jahn–Teller effect [57–59]. The Cu2 site forms four short (1.909–1.990 Å) Cu_2-O bonds and one longer (2.480 Å) Cu2-O bond, thereby forming a CuO_5 [4 + 1]-tetragonal pyramid. There is one longer Cu_2-O_2 contact of 3.121 Å, which complements the pyramid toward the [4 + 1 + 1]-distorted $Cu2O_6$ octahedron. However, the bond valence of the Cu2-O2 bond is rather low (0.02 v.u.), which is below the limit of 0.05 v.u. outlined for meaningful cation–anion bonds [60]. Therefore, this bond is not considered as important for the crystal structure organization.

There are two V^{5+} sites in the crystal structure, both tetrahedrally coordinated by O atoms. Two adjacent $V1O_4$ and $V2O_4$ tetrahedra share the O4 atom to form a V_2O_7 dimer (Figure 2b). The VO_4 tetrahedra are considerably distorted; the degree of distortion is different for the two symmetrically independent tetrahedra, which is quite remarkable. The $V1O_4$ tetrahedron has three shorter V1-O bonds (1.665–1.692 Å) and one longer V1-O bond (1.825 Å), with the longer bond being the O4 atom bridging the V1 and V2 sites. In contrast, the $V2O_4$ contains three comparable V2-O bonds of 1.722–1.763 Å (with the longest bond to the bridging O4 site) and one short V2-O7 bond (1.650 Å). It is of interest to compare the observed distortion of vanadate tetrahedra with those in other $Cu_2V_2O_7$ polymorphs. In blossite, α-$Cu_2V_2O_7$ [38], there is one symmetrically independent VO_4 tetrahedron that has the same type of distortion as the one observed for the V2 site in δ-$Cu_2V_2O_7$: there are three comparable V-O bonds (1.709–1.743 Å) (with the longest to the bridging O atom) and one shorter V-O bond (1.648 Å). The crystal structure of β-$Cu_2V_2O_7$ (ziesite [32]) also contains one V site. The V-O bonds are separated into two groups: two longer bonds

(1.774 Å (to the bridging O atom) and 1.745 Å) and two shorter bonds (1.646 and 1.687 Å). The situation in the crystal structure of γ-$Cu_2V_2O_7$ is very similar to that observed in the δ-polymorph: there are two V sites that have different degrees of distortion: the $V1O_4$ group contains three short V1-O bonds (1.665–1.705 Å) and one longV1-O bond (1.837 Å), whereas the $V2O_4$ group contains one short V2-O bond (1.648 Å) and three longer V2-O bonds (1.727–1.779 Å), with the longest one to the bridging O atom.

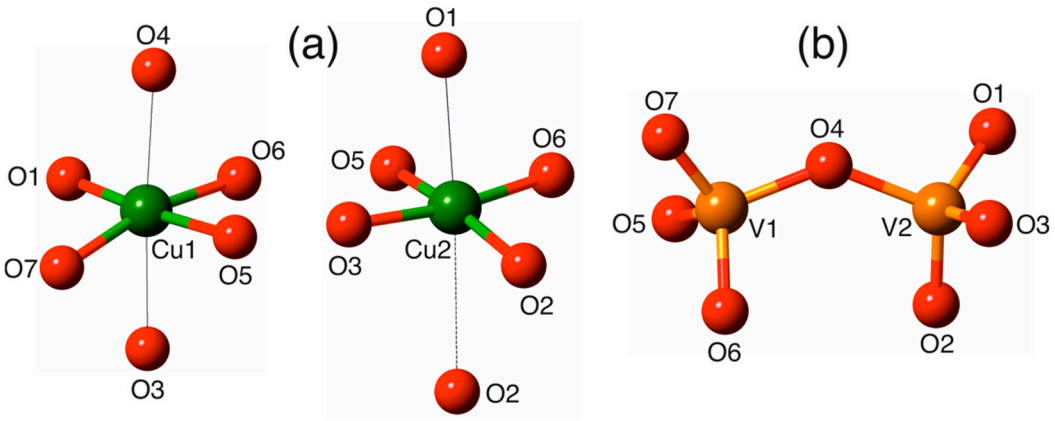

Figure 2. Coordination of Cu^{2+} cations (**a**) and configuration of the V_2O_7 group (**b**) in the crystal structure of δ-$Cu_2V_2O_7$. Legend: Cu: green; V: orange; O: red. The Cu-O bonds with the Cu-O distances in the ranges of < 2.2, 2.2–3.0 and 3.0–3.2 Å are shown as dual-band cylinders, single lines and dashed lines, respectively.

3.2. Structure Description

The polyhedral representation of the crystal structure of δ-$Cu_2V_2O_7$ is shown in Figure 3a. The crystal structure is based upon layers of V_2O_7 dimers of tetrahedra parallel to the (001) plane and interlinked by chains of edge-sharing $Cu1O_6$ and $Cu2O_5$ polyhedra. The chains are parallel to the *a* axis and are arranged into layers also parallel to the (001) plane. Figure 3b shows the arrangement of the chains in a ball-and-stick representation. The CuO_4 squares formed by short (<2.0 Å) Cu-O bonds share O-O edges to form the [$Cu2O_6$] dimers that are further linked by sharing O-O edges that involve apical O atoms in both $Cu1O_6$ octahedral and $Cu2O_5$ tetragonal pyramids. The adjacent chains are linked by long and weak Cu2-O2 interactions (3.121 Å), so that double chains or ribbons are formed. The formation of dimers of strongly bonded CuO_4 squares is an important feature of δ-$Cu_2V_2O_7$, which is also shared by the β- and γ-polymorphs, but not by the *α*-polymorph (see below).

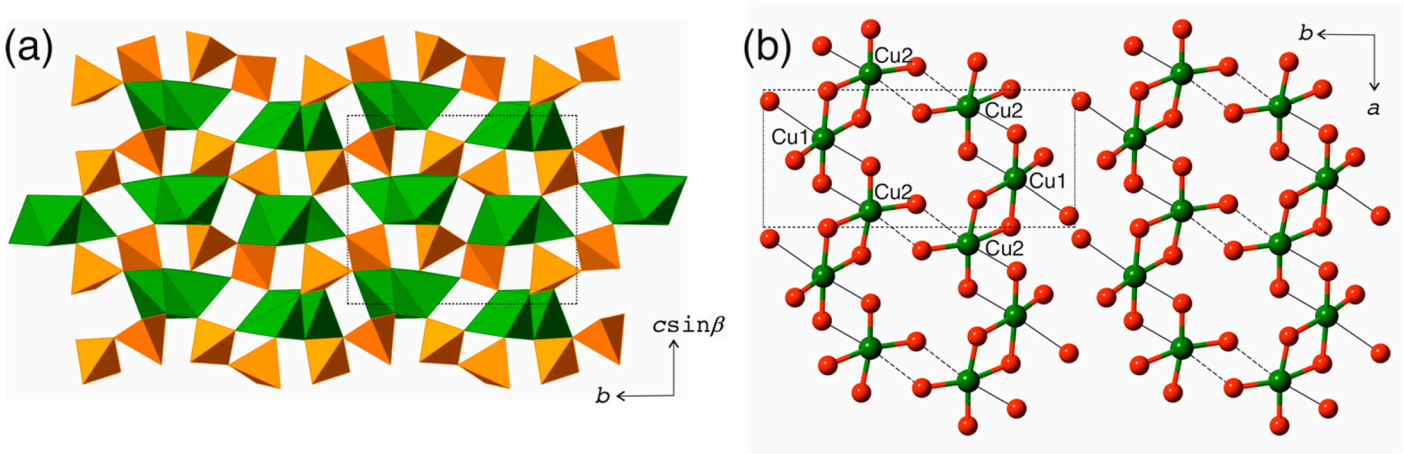

Figure 3. The crystal structure of δ-$Cu_2V_2O_7$ in polyhedral representation (**a**) and the arrangement of the chains of $Cu1O_6$ and $Cu2O_5$ polyhedra within the (001) plane (**b**). Legend as in Figure 2.

4. Discussion

4.1. Structure Comparison of the $Cu_2V_2O_7$ Polymorphs

The crystal structure of δ-$Cu_2V_2O_7$ is closely related to those of three other polymorphs. The general feature of the four crystal structures is that they are based upon layers of V_2O_7 groups interlinked by chains of CuO_n coordination polyhedra (n = 5, 6). However, the details of the interlinkage differ from structure to structure. Below, we outline the basic principles underlying the structural architectures of the three other $Cu_2V_2O_7$ polymorphs in their comparison with δ-$Cu_2V_2O_7$.

In the crystal structure of blossite, α-$Cu_2V_2O_7$ [38], there is one independent Cu site that forms four strong (1.880–1.971 Å) Cu-O bonds complemented by a longer (2.542 Å) Cu-O bond (Figure 4a). The CuO_4 configuration consisting of short Cu-O bonds is a strongly compressed tetrahedron with the O-Cu-O angles between the opposite Cu-O bonds equal to 146 and 159° (the ideal tetrahedron assumes the value of 109.5°). The [4+1] coordination polyhedron is intermediate between a tetragonal pyramid and a trigonal bipyramid and has another long Cu-O contact of 3.025 Å. In blossite, the CuO_5 polyhedra share edges to form chains arranged in layers parallel to the (100) plane (Figure 4b). The chains in the adjacent layers run parallel to [011] and [01$\bar{1}$] (i.e., the chains in the adjacent layers are oriented crosswise) (Figure 4c). Within the chains, the strong CuO_4 tetrahedral configurations share corners so that the Cu···Cu distances are all equal to 3.146 Å.

By analogy with blossite, the crystal structure of ziesite, β-$Cu_2V_2O_7$, contains one independent Cu site coordinated by five O atoms to form a [4 + 1]-distorted CuO_5 tetragonal pyramid (Figure 5a) consisting of CuO_4 squares complemented by a longer (2.265 Å) Cu-O bond. Two CuO_4 squares share an O-O edge to form [Cu_2O_6] dimers, similar to those observed in δ-$Cu_2V_2O_7$. The dimers are further linked by sharing O-O edges involving apical O atoms of the CuO_5 pyramid to form chains arranged into layers parallel to the (001) plane (Figure 5b). As in blossite, the Cu-O chains in the adjacent layers are oriented crosswise and run parallel to [110] and [1$\bar{1}$0] (Figure 5c). Within the chains, the Cu···Cu distances are equal to 2.955 and 3.255 Å, and the shorter and longer contacts alternate.

The crystal structure of γ-$Cu_2V_2O_7$ contains two Cu sites. The Cu1 site is coordinated [4 + 2]-octahedrally with the seventh Cu···O contact equal to 3.182 Å (Figure 6a), whereas the Cu2 coordination is a [4 + 1]-distorted tetragonal pyramid (Figure 6b). There are two symmetrically independent layers of Cu-O chains based upon $Cu1O_6$ and $Cu2O_5$ coordination polyhedra (Figure 6c,d). In both layers, the chains are parallel to the *a* axis. Within the chains, the CuO_4 squares formed by short Cu-O bonds share edges to form [Cu_2O_6] dimers in the same fashion as observed in β- and δ-polymorphs. The linkage of dimers occurs via O-O edges that involve apical O atoms of the CuO_n polyhedra (n = 5, 6). As a result, the Cu···Cu distances are split into two groups: shorter (2.986 and 2.969 Å for Cu1 and Cu2, respectively) and longer (3.200 and 3.113 Å for Cu1 and Cu2, respectively) ones.

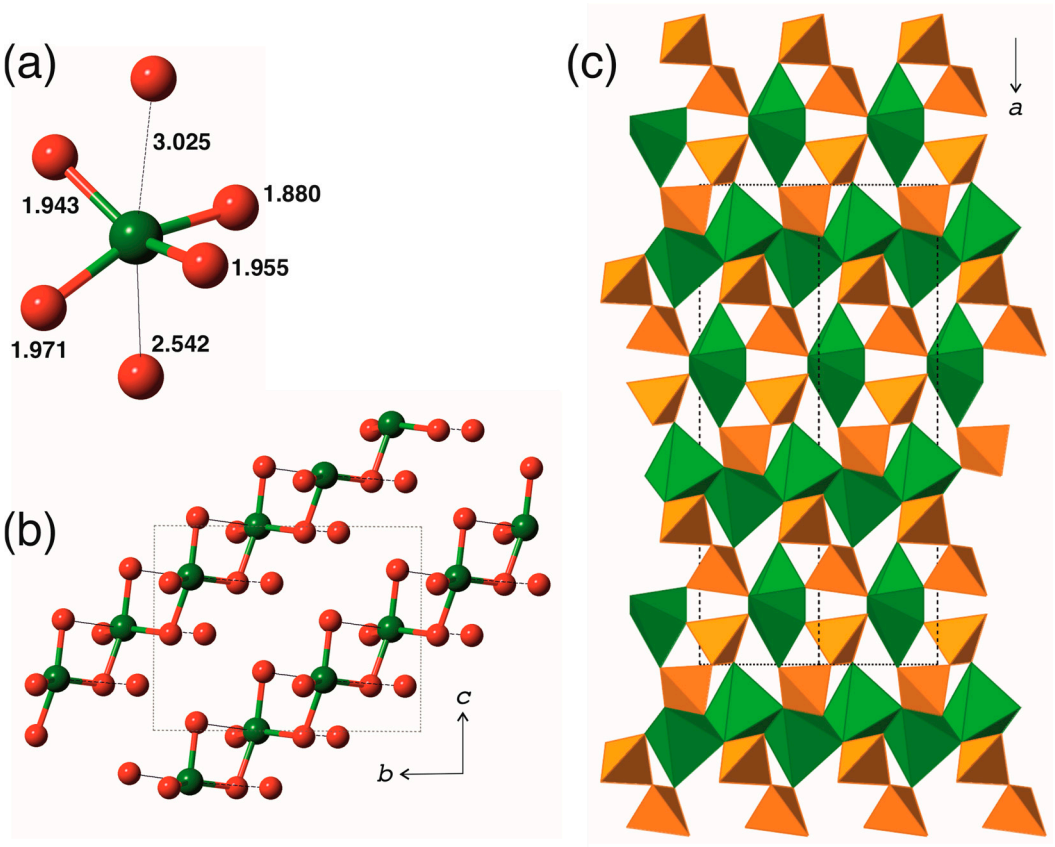

Figure 4. The crystal structure of blossite, α-$Cu_2V_2O_7$: the Cu coordination (**a**), the layer of Cu-O chains (**b**), and the projection of the crystal structure along [01$\bar{1}$] (**c**). Legend as in Figure 2.

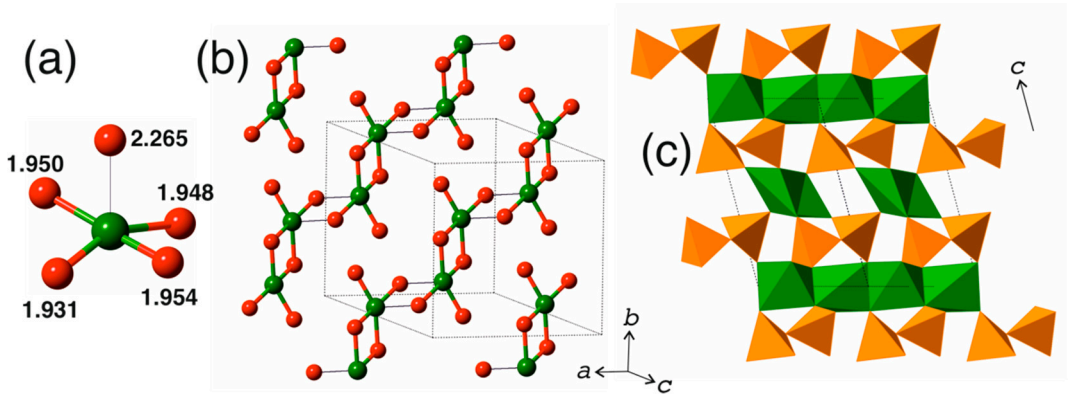

Figure 5. The crystal structure of ziesite, β-$Cu_2V_2O_7$: the Cu coordination (**a**), the layer of Cu-O chains (**b**), and the projection of the crystal structure along [1$\bar{1}$0] (**c**). Legend as in Figure 2.

The structural classification of $Cu_2V_2O_7$ polymorphs can be obtained by considering the mutual orientations of the Cu-O chains in the structure, on the one hand, and the mutual orientations of the V_2O_7 groups, on the other hand. Figure 7 shows a representation of the $Cu_2V_2O_7$ crystal structures in terms of Cu-Cu and V-V graphs, where the vertices correspond to the positions of Cu and V atoms, respectively. The two adjacent Cu atoms are linked by dual-banded cylinder and single lines if the Cu···Cu distances are in the ranges 2.9–3.0 and 3.1–3.2 Å, respectively. The V-V links correspond to the V···V distances in the pyrovanadate V_2O_7 groups, which are in the range of 3.2–3.4 Å.

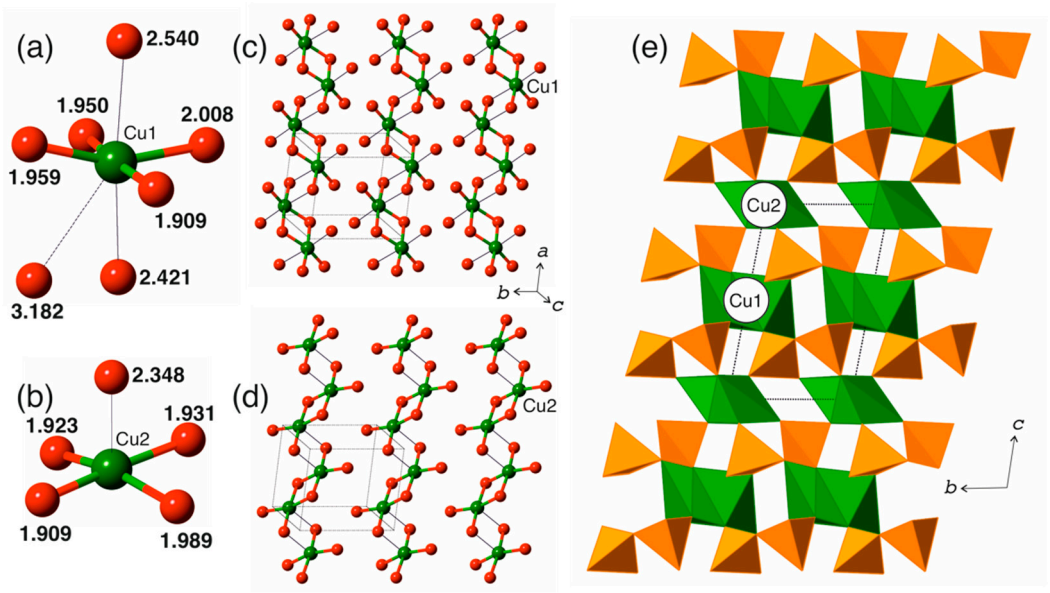

Figure 6. The crystal structure of γ-$Cu_2V_2O_7$: the Cu coordination polyhedra (**a**,**b**), the layers of Cu-O chains (**c**,**d**), and the projection of the crystal structure along the *a* axis (**e**). Legend as in Figure 2.

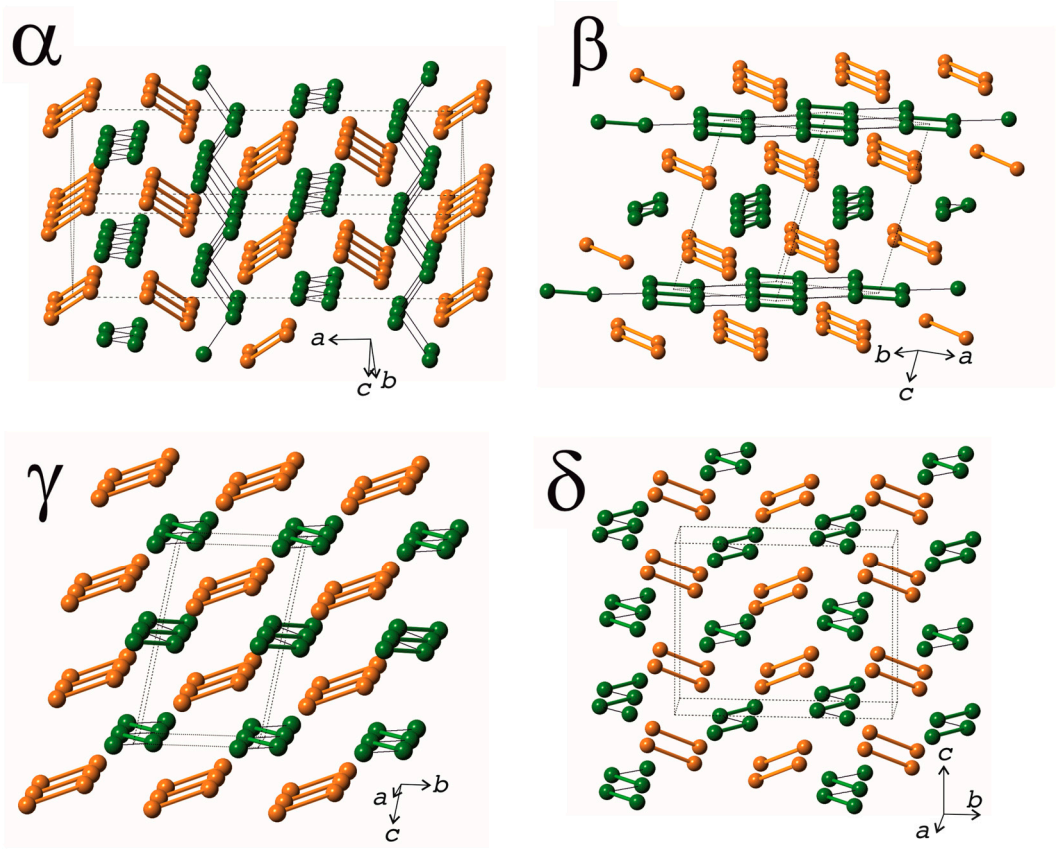

Figure 7. The crystal structures of the four $Cu_2V_2O_7$ polymorphs viewed as consisting of the Cu-Cu and V-V graphs. Legend as in Figure 1. The two adjacent Cu atoms are linked by dual-banded cylinders and single lines if the Cu···Cu distances are in the ranges 2.9–3.0 and 3.1–3.2 Å, respectively. The V-V links correspond to the V···V distances in the divanadate V_2O_7 groups.

In all four polymorphs, the Cu-Cu chains are zigzag-like. Their relative orientations are either parallel (all chains are parallel to one direction (δ- and γ-polymorphs)) or crosswise (the chains run in two different directions (α- and β-polymorphs)). The same type of relations are observed for the V-V dimers: they are either all parallel to each other (β- and

γ-polymorphs) or non-parallel (oriented in two different directions (α- and δ-polymorphs)). The two possible orientations of the Cu-Cu and V-V graphs create four different possible combinations. Figure 8 demonstrates that all four possibilities are realized in the crystal structures of the $Cu_2V_2O_7$ modifications.

The relations between the crystal structures of the γ- and δ-polymorphs can be rationalized in terms of unit cell relations. The unit cell of the δ-phase can be obtained from that of the γ-phase through the application of the [100/020/001] matrix with the subsequent transformation of the resulting triclinic cell into a monoclinic one. Thus, the *b* parameter of the δ-modification is approximately doubled compared to that of the γ-modification. The doubling can be explained by the different orientations of the V_2O_7 groups in the δ-phase versus their parallel orientations in the γ-phase. Hypothetically, the structure of the δ-phase can be obtained from that of the γ-phase by stacking together unit cells of the latter with adjacent unit cells rotated relative to each other by 180° around the *c* axis. Note that the different stackings of the V_2O_7 groups in the two polymorphs result in different coordination environments of the Cu^{2+} cations.

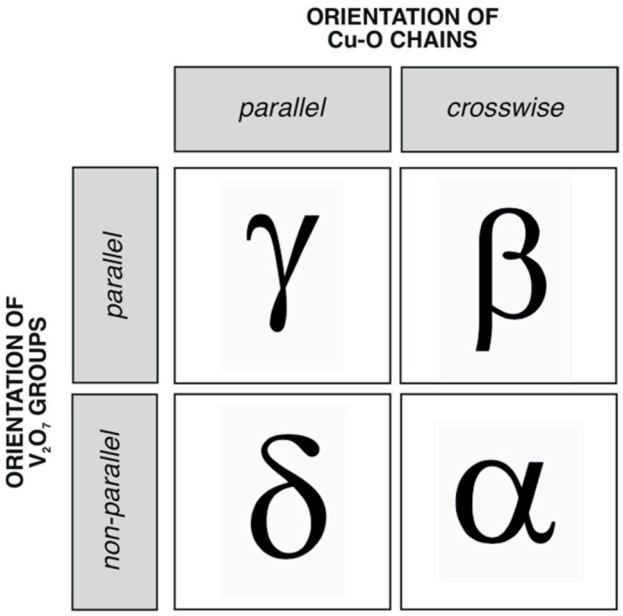

Figure 8. The structural classification scheme for the four $Cu_2V_2O_7$ polymorphs according to the mutual orientations of Cu-O chains and V_2O_7 groups.

4.2. Stability and Nomenclature of the $Cu_2V_2O_7$ Polymorphs

The earlier study of the CuO-V_2O_5 system by Brisi and Molinari [33] identified α- and β-$Cu_2V_2O_7$ as low- and high-temperature polymorphs, respectively, with the phase transition point at 710 °C. This conclusion was supported by subsequent structural investigations [36–38] and the discovery of ziesite in nature as a metastable phase [30]. The $\alpha \leftrightarrow \beta$ phase transition is reversible, but relatively slow (especially in cooling), due to its reconstructive character that can also be deduced from the crystal chemical analysis given above. Table 5 contains crystallographic information on the reported $Cu_2V_2O_7$ polymorphs and their calculated densities. The low- and high-temperature natures of the α- and β-phases, respectively, are fully supported by their density values, since, in the vast majority of cases, the physical density of the high-temperature phase is lower than that of the low-temperature phase. The metastable character of the β-polymorph was also confirmed by Rotermel' et al. [61].

Clark and Garlick [39] observed the formation of β-$Cu_2V_2O_7$ from a stoichiometric mixture of CuO and V_2O_5 at 500 °C, whereas synthesis at higher temperatures results in the formation of α-$Cu_2V_2O_7$. These observations led Clark and Garlick [39] to conclude that β-$Cu_2V_2O_7$ and not α-$Cu_2V_2O_7$ is a low-temperature modification. The $\beta \rightarrow \alpha$

transition was observed at 605 °C with the subsequent transition to the so-called 'γ-phase' (not identical to the γ-phase reported in [43]) at 705 °C. The crystal structure of this 'γ-phase' or β'-$Cu_2V_2O_7$ was reported by Petrova et al. [40] from the powder diffraction data collected at 740 °C as crystallizing in the same space group (*C*2/*c*) as the β-polymorph. In some aspects, the crystal structure refinement quality for β'-$Cu_2V_2O_7$ is questionable, but its general features coincide with those of the β-modification (ziesite). Slobodin et al. [41] performed differential scanning calorimetry studies and followed the conclusions made in [39] with regard to the nature of the α- and β-phases. However, it is well known that high-temperature phases may form metastably under certain kinetic crystallization regimes, since their lower densities (Table 5) result in lower surface energies and lower energy nucleation barriers in comparison with the thermodynamically stable phases [62]. The β'-phase observed above 712 °C is in fact the high-temperature form of the β-polymorph and therefore should not be considered as a separate $Cu_2V_2O_7$ polymorph.

Table 5. Crystallographic parameters of the $Cu_2V_2O_7$ polymorphs.

Phase	Space Group	*a*, Å	*b*, Å	*c*, Å	*α*, deg	*β*, deg	*γ*, deg	*V*/*Z*, Å^3	ρ_{calc}, g·cm^{-3}	Reference
α	*Fdd*2	20.676	8.392	6.446	90	90	90	139.8	4.049	31
		20.680	8.411	6.448	90	90	90	140.2	4.038	36
		20.645	8.383	6.442	90	90	90	139.4	4.062	38
β	*C*2/*c*	7.686	8.034	10.121	90	110.39	90	146.5	3.865	44
		7.689	8.029	10.107	90	110.25	90	146.4	3.868	32
		7.698	8.031	10.113	90	110.29	90	146.6	3.861	29
β'	*C*2/*c*	7.325 *	8.214 *	10.190 *	90 *	111.78 *	90 *	142.4 *	3.997 *	40
γ	$P\bar{1}$	5.080 **	5.810 **	9.380 **	100.00 **	97.20 **	97.18 **	133.7 **	4.234 **	44
		5.087	5.823	9.402	99.78	97.25	97.20	134.6	4.206	43
δ	$P2_1/n$	5.068	11.422	9.446	90	97.10	90	135.7	4.173	This work

* Data at 740 °C. ** Data at 0.40 GPa.

Thus, we suggest that the temperature stability fields of the $Cu_2V_2O_7$ polymorphs at ambient pressures are the same as suggested previously [33–38]: the α- and β-phases are the low- and high-temperature modifications, respectively.

On the basis of the density values of the δ- and γ-polymorphs (Table 5), it can be proposed that both these phases are high-pressure $Cu_2V_2O_7$ modifications. The formation of γ-$Cu_2V_2O_7$ was observed under the compression of β-$Cu_2V_2O_7$ to 0.40 GPa [44], which supports this conclusion. The nature of the δ-polymorph remains unclear. However, it can be hypothesized that it may form under higher pressures than γ-$Cu_2V_2O_7$, or through other pathways (e.g., by the compression of the α-polymorph).

4.3. Structural Complexity

The structural complexity parameters for different $Cu_2V_2O_7$ polymorphs were studied using the information theoretical approach introduced in [63,64]. The two basic complexity parameters are the Shannon information amounts per atom ($^{str}I_G$) and per unit cell ($^{str}I_{G,total}$) that were calculated using the following equations:

$$^{str}I_G = -\sum_{i=1}^{k} p_i \log_2 p_i \text{ (bit/atom)}, \quad (1)$$

$$^{str}I_{G,total} = -v\sum_{i=1}^{k} p_i \log_2 p_i \text{ (bit/cell)}, \quad (2)$$

where *k* is the number of different crystallographic orbits (Wyckoff sites) in the structure and p_i is the random choice probability for an atom from the *i*th crystallographic orbit; that is,

$$p_i = m_i/v, \quad (3)$$

where m_i is a multiplicity of a crystallographic orbit (i.e., the number of atoms of a specific Wyckoff site in the reduced unit cell) and v is the total number of atoms in the reduced unit cell. The complexity parameters are provided in Table 6.

There is a tendency of decreasing structural complexity with increasing temperature [64,65]. In the case of the $Cu_2V_2O_7$ polymorphs, the structural information is identical for the low- and high- temperature phases (α- and β-phases, respectively). Note that the overall symmetry at the critical point decreases from orthorhombic (*Fdd*2) to monoclinic (*C*2/*c*), despite the general tendency of increasing symmetry under increasing temperature [66]. However, the structural complexity remains constant, which points out that the information-based parameters are more sensitive symmetry indicators than point-group symmetry.

The δ- and γ-polymorphs are more complex than the ambient-pressure α- and β-polymorphs, which also corresponds to the general tendency of increasing order under increasing pressure [67]. The δ-phase first reported herein is the most complex among the known $Cu_2V_2O_7$ polymorphs, providing additional support for the hypothesis about its high-pressure nature.

Table 6. Information-based structural complexity parameters for $Cu_2V_2O_7$ polymorphs.

Polymorph	System	Space Group	${}^{str}I_G$, Bit/Atom	${}^{str}I_{G,total}$, Bit/Cell
α	Orthorhombic	*Fdd*2	2.550	56.107
β	Monoclinic	*C*2/*c*	2.550	56.107
γ	Triclinic	$P\bar{1}$	3.459	76.107
δ	Monoclinic	$P2_1/n$	3.459	152.215

5. Conclusions

In conclusion, we report the synthesis and crystal structure of the new $Cu_2V_2O_7$ polymorph, the δ-phase, obtained by chemical vapor transport reactions. Its crystal structure has many similarities to those of the known modifications of copper divanadate, but it is generally new. The crystal chemical analysis of the four known $Cu_2V_2O_7$ phases indicates that they are based upon layers of V_2O_7 groups interlinked by layers consisting of chains of CuO_n coordination polyhedra (n = 5, 6). The crystal structures can be classified according to mutual relations between the Cu-O chains, on the one hand, and the V_2O_7 groups, on the other hand. The analysis of the literature data and physical density values suggests that, at ambient pressure, α- and β-$Cu_2V_2O_7$ are the low- and high-temperature polymorphs, respectively, with the phase transition point at 705–710 °C. The β-phase may form metastably under temperatures below 560 °C and, under heating, transform into the stable α-phase at 605 °C. The δ- and γ-polymorphs have the highest densities and most probably are the high-pressure phases. The structural complexity relations among the polymorphs correspond to the sequence α = β < γ < δ; i.e., the δ phase described herein possesses the highest complexity, which supports the hypothesis about its stability under high-pressure conditions.

Author Contributions: Conceptualization, S.V.K.; methodology, I.V.K. and S.V.K.; formal analysis, I.V.K. and S.V.K.; investigation, I.V.K. and S.V.K.; writing—original draft preparation, S.V.K.; writing—review and editing, S.V.K. and I.V.K.; funding acquisition, S.V.K. All authors have read and agreed to the published version of the manuscript.

Funding: This research was funded by the Russian Science Foundation, grant 24-17-00083.

Data Availability Statement: The original contributions presented in the study are included in the article, further inquiries can be directed to the corresponding author.

Acknowledgments: The X-ray diffraction measurements were performed at the Centre for the Collective Use of Equipment of the Kola Science Centre, Russian Academy of Sciences.

Conflicts of Interest: The authors declare no conflicts of interest.

References

1. Guo, W.; Chemelewski, W.D.; Mabayoje, O.; Xiao, P.; Zhang, Y.; Mullins, C.B. Synthesis and Characterization of CuV_2O_6 and $Cu_2V_2O_7$: Two Photoanode Candidates for Photoelectrochemical Water Oxidation. *J. Phys. Chem. C* **2015**, *119*, 27220–27227.
2. Kim, M.; Joshi, B.; Yoon, H.; Ohm, T.Y.; Kim, K.; Al-Deyab, S.S.; Yoon, S.S. Electrosprayed Copper Hexaoxodivanadate (CuV_2O_6) and Pyrovanadate ($Cu_2V_2O_7$) Photoanodes for Efficient Solar Water Splitting. *J. Alloys Compds* **2017**, *708*, 444–450.
3. Gadiyar, C.; Strach, M.; Schouwink, P.; Loiudice, A.; Buonsanti, R. Chemical Transformations at the Nanoscale: Nanocrystal-Seeded Synthesis of β-$Cu_2V_2O_7$ with Enhanced Photoconversion Efficiencies. *Chem. Sci.* **2018**, *9*, 5658–5665.
4. Wiktor, J.; Reshetnyak, I.; Strach, M.; Scarongella, M.; Buonsanti, R.; Pasquarello, A. Sizable Excitonic Effects Undermining the Photocatalytic Efficiency of β-$Cu_2V_2O_7$. *J. Phys. Chem. Lett.* **2018**, *9*, 5698–5703.
5. Hassan, A.; Iqbal, T.; Tahir, M.B.; Afsheen, S. A Review on Copper Vanadate-Based Nanostructures for Photocatalysis Energy Production. *Int. J. Energy Res.* **2019**, *43*, 9–28.
6. Rao, M.P.; Akhila, A.K.; Wu, J.J.; Asiri, A.M.; Anandan, S. Synthesis, Characterization and Adsorption Properties of $Cu_2V_2O_7$ Nanoparticles. *Solid State Sci.* **2019**, *92*, 13–23.
7. Guo, W.; Lian, X.; Nie, Y.; Hu, M.; Wu, L.; Gao, H.; Wang, T. Facile Growth of β-$Cu_2V_2O_7$ Thin Films and Characterization for Photoelectrochemical Water Oxidation. *Mater. Lett.* **2020**, *258*, 126842.
8. Camargo, L.P.; Lucilha, A.C.; Gomes, G.A.B.; Liberatti, V.R.; Andrello, A.C.; da Silva, P.R.C.; Dall'Antonia, L.H. Copper Pyrovanadate Electrodes Prepared by Combustion Synthesis: Evaluation of Photoelectroactivity. *J. Solid State Electrochem.* **2020**, *24*, 1935–1950.
9. Song, A.; Chemseddine, A.; Ahmet, I.Y.; Bogdanoff, P.; Friedrich, D.; Abdi, F.F.; Berglund, S.P.; van de Krol, R. Evaluation of Copper Vanadate (β-$Cu_2V_2O_7$) as a Photoanode Material for Photoelectrochemical Water Oxidation. *Chem. Mater.* **2020**, *32*, 2408–2419.
10. Muthamizh, S.; Yesuraj, J.; Jayavel, R.; Contreras, D.; Arul Varman, K.; Mangalaraja, R.V. Microwave Synthesis of β-$Cu_2V_2O_7$ Nanorods: Structural, Electrochemical Supercapacitance, and Photocatalytic Properties. *J. Mater. Sci.: Mater. Electr.* **2021**, *32*, 2744–2756.
11. Keerthana, S.P.; Yuvakkumar, R.; Kumar, P.S.; Ravi, G.; Velauthapillai, D. Surfactant Induced Copper Vanadate (β-$Cu_2V_2O_7$, $Cu_3V_2O_8$) for Different Textile Dyes Degradation. *Environ. Res.* **2022**, *211*, 112964.
12. Moussaid, D.; Khallouk, K.; El Khalfaouy, R.; Tagnaouti Moumnani, F.; Kherbeche, A.; Barakat, A. Solution Combustion Synthesis of β-$Cu_2V_2O_7$ Nanoparticles: Photocatalytic Degradation of Crystal Violet under UV and Visible Light Illumination. *React. Kin. Mech. Catal.* **2022**, *135*, 2797–2812.
13. Musuvadhi Babulal, S.; Anupriya, J.; Chen, S.M. Self Assembled Three Dimensional β-$Cu_2V_2O_7$ Hierarchical Flower Decorated Porous Carbon: An Efficient Electrocatalyst for Flutamide Detection in Biological and Environmental Samples. *Chemosphere* **2022**, *303*, 135203.
14. Ponomarenko, L.A.; Vasil'ev, A.N.; Antipov, E.V.; Velikodny, Y.A. Magnetic Properties of $Cu_2V_2O_7$. *Physica B: Cond. Mat.* **2000**, *284–288*, 1459–1460.
15. Yashima, M.; Suzuki, R.O. Electronic Structure and Magnetic Properties of Monoclinic β-$Cu_2V_2O_7$: A GGA+*U* Study. *Phys. Rev. B* **2009**, *79*, 125201.
16. Tsirlin, A.A.; Janson, O.; Rosner, H. β-$Cu_2V_2O_7$: A Spin-1/2 Honeycomb Lattice System. *Phys. Rev. B* **2010**, *82*, 144416.
17. Janson, O.; Tsirlin, A.A.; Sichelschmidt, J.; Skourski, Y.; Weickert, F.; Rosner, H. Long-Range Superexchange in $Cu_2A_2O_7$ (A = P, As, V) as a Key Element of the Microscopic Magnetic Model. *Phys. Rev. B* **2011**, *83*, 094435.
18. Sánchez-Andújar, M.; Yáñez-Vilar, S.; Mira, J.; Biskup, N.; Rivas, J.; Castro-García, S.; Señarís-Rodríguez, M.A. Role of the Magnetic Ordering on the Dielectric Response of $M_2V_2O_7$ (M = Co and Cu) Divanadates. *J. Appl. Phys.* **2011**, *109*, 054106.
19. Gitgeatpong, G.; Zhao, Y.; Avdeev, M.; Piltz, R.O.; Sato, T.J.; Matan, K. Magnetic Structure and Dzyaloshinskii-Moriya Interaction in the S = 1/2 Helical-Honeycomb Antiferromagnet a-$Cu_2V_2O_7$. *Phys. Rev. B* **2015**, *92*, 024423.
20. Banerjee, A.; Sannigrahi, J.; Bhowal, S.; Dasgupta, I.; Majumdar, S.; Walker, H.C.; Bhattacharyya, A.; Adroja, D.T. Spin Wave Excitations in the Pyrovanadate a-$Cu_2V_2O_7$. *Phys. Rev. B* **2016**, *94*, 144426.
21. Bhowal, S.; Sannigrahi, J.; Majumdar, S.; Dasgupta, I. A Comparative Study of Electronic, Structural, and Magnetic Properties of α-, β-, and γ- $Cu_2V_2O_7$. *Phys. Rev. B* **2017**, *95*, 075110.
22. Gitgeatpong, G.; Suewattana, M.; Zhang, S.; Miyake, A.; Tokunaga, M.; Chanlert, P.; Kurita, N.; Tanaka, H.; Sato, T.J.; Zhao, Y.; et al. High-Field Magnetization and Magnetic Phase Diagram of a-$Cu_2V_2O_7$. *Phys. Rev. B* **2017**, *95*, 245119.
23. Ruan, M.Y.; Ouyang, Z.W.; Sun, Y.C.; Xia, Z.C.; Rao, G.H.; Chen, H.S. Examining Magnetic Models and Anisotropies in β-$Cu_2V_2O_7$ by High-Frequency ESR. *Appl. Magn. Res.* **2017**, *48*, 423–433.
24. Kunwar, H.S.; Isha; Yogi, A.K.; De, B.K.; Dwij, V.; Gupta, M.K.; Mittal, R.; Venkatesh, R.; Chaudhary, R.J.; Vedpathak, M.; et al. Raman Scattering of Spin-1/2 Mixed-Dimensionality Antiferromagnetic a-$Cu_2V_2O_7$. *Phys. Rev. B* **2024**, *109*, 054310.
25. Sannigrahi, J.; Bhowal, S.; Giri, S.; Majumdar, S.; Dasgupta, I. Exchange-Striction Induced Giant Ferroelectric Polarization in Copper-Based Multiferroic Material a-$Cu_2V_2O_7$. *Phys. Rev. B* **2015**, *91*, 220407.

26. Shiomi, Y.; Takashima, R.; Okuyama, D.; Gitgeatpong, G.; Piyawongwatthana, P.; Matan, K.; Sato, T.J.; Saitoh, E. Spin Seebeck Effect in the Polar Antiferromagnet a-$Cu_2V_2O_7$. *Phys. Rev. B* **2017**, *96*, 180414.
27. Zhang, J.T.; Wang, J.L.; Ji, C.; Guo, B.X.; Xia, W.S.; Lu, X.M.; Zhu, J.S. Magnetism and Spin-Driven Ferroelectricity in the Multiferroic Material a-$Cu_2V_2O_7$. *Phys. Rev. B* **2017**, *96*, 165132.
28. Zhang, N.; Li, L.; Wu, M.; Li, Y.; Feng, D.; Liu, C.; Mao, Y.; Guo, J.; Chao, M.; Liang, E. Negative Thermal Expansion and Electrical Properties of α-$Cu_2V_2O_7$. *J. Eur. Ceram. Soc.* **2016**, *36*, 2761–2766.
29. Wang, H.; Yang, M.; Chao, M.; Guo, J.; Gao, Q.; Jiao, Y.; Tang, X.; Liang, E. Negative Thermal Expansion Property of β-$Cu_2V_2O_7$. *Solid State Ionics* **2019**, *343*, 115086.
30. Hughes, J.M.; Birnie, R.W. Ziesite, β-$Cu_2V_2O_7$, a New Copper Vanadate and Fumarole Temperature Indicator. *Amer. Miner.* **1980**, *65*, 1146–1149.
31. Robinson, P.D.; Hughes, J.M.; Malinconico, M.L. Blossite, Alpha -$Cu^{2+}{}_2V^{5+}{}_2O_7$, a New Fumarolic Sublimate from Izalco Volcano, El Salvador. *Amer. Miner.* **1987**, *72*, 397–400.
32. Hughes, J.M.; Brown, M.A. The crystal structure of ziesite, β-$Cu_2V_2O_7$, a thortveitite-type structure with a non-linear X-O-X inter-tetrahedral bond. *N. Jb. Miner. Mh.* **1989**, *1989*, 41–47.
33. Brisi, C.; Molinari, A. Il sistema ossido ramicoanidride vanadica. *Ann. Chim.* **1958**, *48*, 263–269.
34. Fleury, P. Sur le systéme CuO-V_2O_5. *C.R Acad. Sci. Paris Ser. C* **1966**, *263*, 1375–1377.
35. Fleury, P. Etudes sur les systémes V_2O_5-CuO ou Ag_2O ou Tl_2O_3 et sur les combinaisons interoxydes comespondantes. *Rev. Chim. Mineral.* **1969**, *6*, 819–851.
36. Mercurio-Lavaud, D.; Frit, B. Structure cristalline de la variété basse température du pyrovanadate de cuivre: $Cu_2V_2O_7$ α. *Acta Crystallogr. B* **1973**, *29*, 2737–2741.
37. Mercurio-Lavaud, D.; Frit, M.B. Structure cristalline de la variété haute température du pyrovanadate de cuivre: $Cu_2V_2O_7$. *C. R. Acad. Sci. Paris* **1973**, *277C*, 1101–1104.
38. Calvo, C.; Faggiani, R. α Cupric Divanadate. *Acta Crystallogr. B* **1975**, *31*, 603–605.
39. Clark, G.M.; Garlick, R. Formation and Properties of Copper(II) Divanadate(V). *J. Inorg. Nucl. Chem.* **1978**, *40*, 1347–1349.
40. Petrova, S.A.; Zakharov, R.G.; Rotermel', M.V.; Krasnenko, T.I.; Vatolin, N.A. A New High-Temperature Modification of Copper Pyrovanadate. *Dokl. Chem.* **2005**, *400*, 30–33.
41. Slobodin, B.V.; Surat, L.L.; Samigullina, R.F. Polymorphism in Copper Pyrovanadate. *Russ. J. Inorg. Chem.* **2009**, *54*, 797–802.
42. Slobodin, B.V.; Samigullina, R.F. Thermoanalytical Study of the Polymorphism and Melting Behavior of $Cu_2V_2O_7$. *Inorg. Mater.* **2010**, *46*, 196–200.
43. Krivovichev, S.V.; Filatov, S.K.; Cherepansky, P.N.; Armbruster, T.; Pankratova, O.Y. Crystal structure of γ-$Cu_2V_2O_7$ and its comparison to blossite (α-$Cu_2V_2O_7$) and ziesite (β-$Cu_2V_2O_7$). *Can. Miner.* **2005**, *43*, 671–677.
44. Turnbull, R.; González-Platas, J.; Rodríguez, F.; Liang, A.; Popescu, C.; He, Z.; Santamaría-Pérez, D.; Rodríguez-Hernández, P.; Muñoz, A.; Errandonea, D. Pressure-Induced Phase Transition and Band Gap Decrease in Semiconducting β-$Cu_2V_2O_7$. *Inorg. Chem.* **2022**, *61*, 3697–3707.
45. Kornyakov, I.V.; Krivovichev, S.V.; Gurzhiy, V.V.; Leoni, M. ε-$RbCuCl_3$, a new polymorph of rubidium copper trichloride: Synthesis, structure and structural complexity. *Acta Crystallogr. C* **2018**, *74*, 529–533.
46. Integrated X-ray Powder Diffraction Software PDXL. *Rigaku J.* **2010**, *26*, 23–27.
47. Gates-Rector, S.; Blanton, T. The Powder Diffraction File: A Quality Materials Characterization Database. *Powder Diffr.* **2019**, *34*, 352–360.
48. Zagorac, D.; Müller, H.; Ruehl, S.; Zagorac, J.; Rehme, S. Recent developments in Inorganic Crystal Structure Database: Theoretical crystal structure data and related features. *J. Appl. Crystallogr.* **2019**, *52*, 918–925.
49. Coelho, A.A. TOPAS and TOPAS-Academic: An optimization program integrating computer algebra and crystallographic objects written in C++. *J. Appl. Crystallogr.* **2018**, *51*, 210–218.
50. Savariault, J.-M.; Galy, J. Synthesis and structural investigation of a new potassium vanadium oxide bronze: ϱ-$K_{0.50}V_2O_5$. *J. Solid State Chem.* **1992**, *101*, 119–127.
51. Martin, F.-D.; Müller-Buschbaum, H. Zur Kenntnis von $K_4CuV_5O_{15}Cl$. *Zeitschrift Naturforschung B.* **1994**, *49*, 1459–1462.
52. Haase, A.; Brauer, G. Vanadium oxychloride. *Acta Cryst.* **1975**, *B31*, 2521–2522.
53. Agilent Technologies. *CrysAlisPro*, Version 1.171.36.20; Agilent Technologies: Santa Clara, CA, USA, 2012.
54. Sheldrick, G.M. A short history of SHELX. *Acta Crystallogr.* **2008**, *A64*, 112–116.
55. Dolomanov, O.V.; Bourhis, L.J.; Gildea, R.J.; Howard, J.A.K.; Puschmann, H. OLEX2: A complete structure solution, refinement and analysis program. *J. Appl. Crystallogr.* **2009**, *42*, 339–341.
56. Gagné, O.C.; Hawthorne, F.C. Comprehensive Derivation of Bond-Valence Parameters for Ion Pairs Involving Oxygen. *Acta Crystallogr. B* **2015**, *71*, 562–578.
57. Jahn, H.A.; Teller, E. Stability of polyatomic molecules in degenerate electronic states. *Proc. Roy. Soc. Ser. A.* **1937**, *161*, 220–235.
58. Hathaway, B.J. A new look at the stereochemistry and electronic properties of complexes of the copper(II) ion. In *Complex Chemistry. Structure and Bonding;* Emsley, J., Ernst, R.D., Hathaway, B.J., Warren, K.D., Eds.; Springer: Berlin/Heidelberg, Germany, 1984; Volume 57, pp. 55–118.
59. Burns, P.C.; Hawthorne, F.C. Static and dynamic Jahn-Teller effects in Cu^{2+} oxysalt minerals. *Can. Mineral.* **1996**, *34*, 1089–1105.
60. Brown, I.D. *The Chemical Bond in Inorganic Chemistry. The Bond-Valence Model*; Oxford University Press: Oxford, UK, 2016.

61. Rotermel', M.V.; Krasnenko, T.I.; Petrova, S.A.; Zakharov, R.G. Thermally Activated Transformations in Stable and Metastable Copper(II) Pyrovanadate Polymorphs. *Russ. J. Inorg. Chem.* **2009**, *54*, 22–26.
62. Krivovichev, S.V. Metastable Crystallization and Structural Complexity of Minerals. *Dokl. Earth Sci.* **2022**, *507*, 1040–1043.
63. Krivovichev, S.V. Topological complexity of crystal structures: Quantitative approach. *Acta Crystallogr*. **2012**, *A68*, 393–398.
64. Krivovichev, S.V. Structural complexity of minerals: Information storage and processing in the mineral world. *Miner. Mag.* **2013**, *77*, 275–326.
65. Krivovichev, S.V.; Krivovichev, V.G.; Hazen, R.M.; Aksenov, S.M.; Avdontceva, M.S.; Banaru, A.M.; Gorelova, L.A.; Ismagilova, R.M.; Kornyakov, I.V.; Kuporev, I.V.; Morrison, S.M.; Panikorovskii, T.L.; Starova, G.L. Structural and chemical complexity of minerals: An update. *Mineral. Mag*. **2022**, *86*, 183–204.
66. Filatov, S.K. General Concept of Increasing Crystal Symmetry with an Increase in Temperature. *Crystallogr. Rep.* **2011**, *56*, 953–961.
67. Hazen, R.M.; Navrotsky, A. Effects of Pressure on Order-Disorder Reactions. *Amer. Miner.* **1996**, *81*, 1021–1035.

Disclaimer/Publisher's Note: The statements, opinions and data contained in all publications are solely those of the individual author(s) and contributor(s) and not of MDPI and/or the editor(s). MDPI and/or the editor(s) disclaim responsibility for any injury to people or property resulting from any ideas, methods, instructions or products referred to in the content.